Unsteady Aerodynamics and Wake Structures of Butterfly in Forward Flight

Zhipeng Lou¹ and Chengyu Li² Department of Mechanical Engineering, Villanova University, Villanova, PA 19085

The unsteady aerodynamics mechanisms, such as coupled wing-body aerodynamics, are believed to benefit the flapping flight of the insects. The butterfly takes more advantage of it than other insects because of its unique wing-body morphology and periodical body rotational motion. Our study conducted 3D reconstruction of a monarch butterfly and we adopted an in-house three-dimensional immersed-boundary-method Navier-Stokes equation solver to simulate the natural forward flight of the butterfly. By comparing the simulation with and without the influence of the body, we present a parametric study that proves the coupled wing-body interaction can improve the thrust-to-power ratio. During the upstroke the thrust is improved by 10%. During the upstroke, a posterior body vortex (PBV) that is attached beneath the body is induced by wing motion, which forms a jet flow as upstroke goes on. We visualized wake structures by Q-criterion and observed that the LEV has the strongest circulation at 68% wingspan. The circulation along the leading-edge shows similar trend as the instantaneous lift.

= Wing stroke amplitude

= Wing deviation amplitude

= Wing pitch amplitude

= Reynolds number

v = Reynolds number

= Flapping frequency

t/T = Normalized time

Nomenclature

 F_D = Drag force

 $F_L = \text{Lift force}$

I. Introduction

During a flapping wing flight, the wing motion induces unsteady flow which has been found indispensable. To characterize the unsteady aerodynamics, researcher have developed experimental and numerical methods [1–5]. It has been found the mechanism that how the flapping motion improves the aerodynamic, such as delayed stall, the mechanism that generates sufficient lift to keep an insects aloft [6]. Recent studies have discovered the mechanism that coupled wing-body dynamics enhance the aerodynamics forces and efficiency, which are carried out among many insects, including cicadas [7], fruit fly [8,9], and butterflies [10]. For example, Sridhar et al., demonstrated that the coupled wing-body motion could improve the lift-to-power efficiency, which was relevant to the wing-load and reduced frequency [10]. Other than the parametric studies comparing aerodynamic forced and power with morphological parameters, studies also showed that the wake structures generated from the wing-body interaction could enhance the lift [7,11]. Such lift enhancement was believed to be the result of the wide body shape of the cicada, so the vortices generated by the wing flapping motion were affected by the body when they got close to it. Compared with the body width of cicada that is up to half of the wingspan, the width of the butterfly body is roughly one-tenth to one-fourteenth of the wingspan. It remains unclear if such slimer body of the

¹ Ph.D. student, <u>zlou01@villanova.edu</u>, AIAA Member

² Assistant Professor, chengyu.li@villnoava.edu, AIAA Member

butterfly also has similar effects on the vortex formation. We suspect that such vortex structure caused by wing body coupling may have different effects on the aerodynamic performance. In this study, we conducted 3D reconstructions based on high-speed recording of forward flying monarch butterflies, and we adopted an in-house three-dimensional immersed-boundary-method Navier-Stokes equation solver to simulate the natural forward flight of the butterfly. By comparing the simulations with or without the influence of the body, we show the mechanism how the body impacts the aerodynamics forces produced by wings and how the body effects the vortex generation.

II. Methodology

A. 3D reconstruction of a forward flying butterfly

We recorded the nature flight of a monarch butterfly (Danaus plexippus) using high-speed photography. The butterflies were placed in the laboratory which were expected to fly to a preconstructed filming scene voluntarily. The filming scene consisted of three orthogonal Photron Fastcam SA3 cameras with frame rate of 1000 frame per second and 1024*1024 pixels. In front of the cameras, there were three orthogonal background boards facing them respectively. One flapping period of an individual monarch butterfly was picked for 3D reconstruction whose well-posed upwind surging flight was captured. We did the 3D reconstruction in Autodesk MAYA. We first generated a static template model, then apply kinematics to the model as Figure 1. The forewing and hindwing are modelled as one continuous surface.



Figure 1. The schematic of butterfly model reconstruction. The left half is the computational mesh of the template model and is shown as red lines on the left. The right half is the top view of the monarch butterfly picture.

B. Definition of wing and body kinematics

Figure 2a defines the body Euler angle. The body pitching angle θ_b is defined as the angle between the body center line and the horizontal plane. The body center line is the line between the head and the hinge of body and abdomen. The rolling and the yawing of the body are removed in this study for simplification.

As shown in Figure 2b, the wing kinematics are described in a reference frame based on the stroke plane that fixed to the body. The stroke plane is obtained by the least-square plane of the wing root and wing tip trajectory. The rotation of the wings are governed by stroke angle ψ_w , the deviation angle ϕ_w , and the pitch angle θ_w . The wing stroke angle ψ_w is the angle between the z_w axis and the projection of the root-to-tip line on the stroke plane. The deviation angle ϕ_w is the angle between the root-to-tip line and the stroke plane. The wing pitch angle θ_w is the angle between the wing chord and the stroke plane.

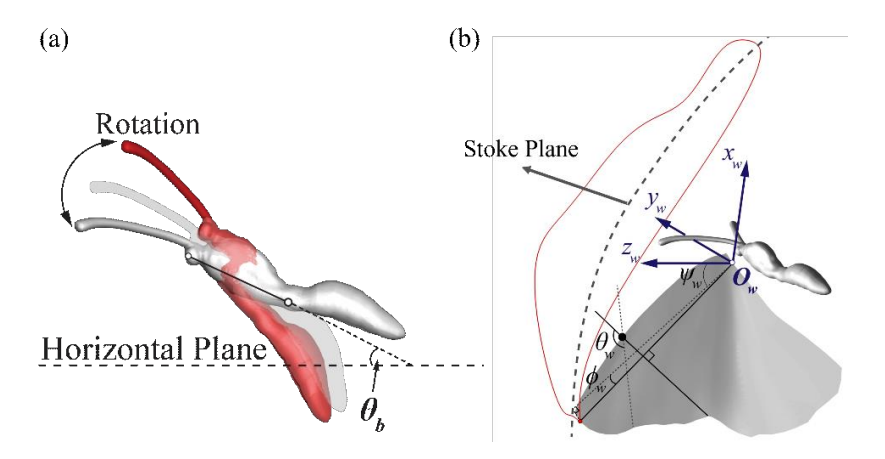


Figure 2. (a) The definition of butterfly wing Euler angles. $x_w y_w z_w$ is a local coordinate system whose origin O_w is located at wing root. The gray dotted line is on the mean stroke plane and crosses the beginning of the upstroke and downstroke.

C. Numerical methods

The numerical simulations use an in-house three-dimensional immersed-boundary-method Navier-Stokes equation solver. The normalized form of the three-dimensional viscous incompressible Navier-Stokes equations are written as Eq. (1) and Eq. (2):

$$\frac{\partial u_i}{\partial x_i} = 0 \tag{1}$$

$$\frac{\partial u_i}{\partial t} + \frac{\partial (u_i u_j)}{\partial x_i} = -\frac{\partial p}{\partial x_i} + \frac{1}{Re} \frac{\partial}{\partial x_i} \left(\frac{\partial u_i}{\partial x_i} \right)$$
 (2)

 u_i (i = 1, 2 and 3) are the velocity components in x, y, and z directions. p is the pressure. The Reynold number is defined by $Re = U_{\infty}R/v$. The characteristic length and time are wingspan (R) and flapping period (T), as shown in Table I.

Table I. Parameters for normalization

Flight speed, U_{∞} [m/s]	Wingspan, R [mm]	Period, T [s]	Kinematics Viscosity, v [m ² /s]	Re
0.967	79.51	0.09	1.56×10^{-5}	4928.6

The present study employs a multi-dimensional "ghost-cell" methodology to impose the boundary conditions on the immersed boundary [12]. This method can be categorized as a discrete forcing approach wherein forcing is directly incorporated into the discretized Navier-Stokes equations. The movement of the immersed boundaries (wings and body) were prescribed according to the image-based reconstruction as described in subsection A. This immersed-boundary-method has successfully been used to simulate insect flights [13–19] and bio-inspired propulsions [20–25]. Validations of the current in-house CFD solver can be found in our previous studies [18,26–30].

The mechanical power consists of aerodynamic power (P_a) and inertial power (P_i) . The aerodynamic power is the power consumption to overcome the air resistance, and the inertial power is consumed to the accelerate wings. They are defined by Eq. (3), Eq. (4) and Eq. (5).

$$P_a = -\iint (\Delta P + \Delta \tau) \vec{u}_c ds \tag{3}$$

$$P_i = \iint \frac{m_w}{S_w} \cdot \frac{d\mathbf{u}_c}{dt} \cdot \mathbf{u}_c ds \tag{4}$$

$$P_{mech} = P_{aero} + P_{iner} \tag{5}$$

 ΔP and $\Delta \tau$ are the pressure difference and shear stress difference between the two sides of the wing surface, respectively; \mathbf{u}_c is cell-centered velocity vector of the triangular element on the wing, s is the area of the triangular element.

D. Simulation setup

The simulation is performed in a 288×176×224 non-uniform cubical Cartesian grid (Figure 3), and the size of the flow region is 15R×15R×15R, where R is the wingspan. The grid consists of three portions of meshes: the inner densest mesh layer, the secondary less dense mesh layer, and the outside coarse layer. The densest mesh layer covers the butterfly model and maximum spacing between adjacent nodes is less than 1.5%R, which is found fine enough for the current study. The secondary less dense layer covers most downstream vortices. For the second layer, the maximum distance among nodes is roughly 2% of the flow region length. The coarser meshes outside are stretched towards the border of the flow region.

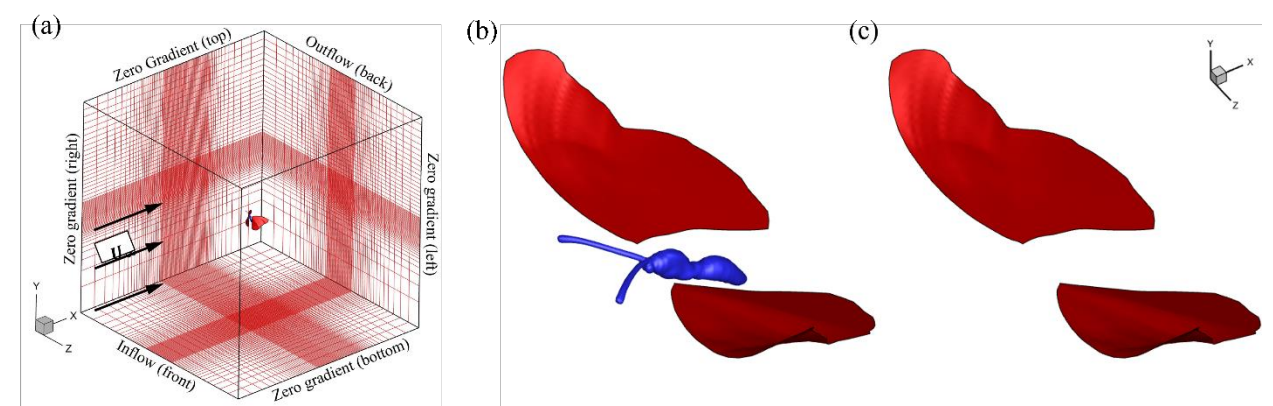


Figure 3. (a) The configuration of the computational mesh (roughly 11 million grids) and boundary conditions. (b) Original model; (c) wing-only model.

To evaluate the wing-body coupling effects, we have run two simulations, an original case (Figure 3b) and a wing-only case (Figure 3c). The wing-only case is the original case without the body while the kinematics of the wings are identical. Since the wing roots are fixed on the body, the wing frame is fixed on the body frame and rotates while the body rotates. For wing-only case, although the body is removed, the rotation of the body frame still exists and remains the same as the original case.

III. Results

In the results section, the simulation results are provided, including the kinematics, the aerodynamic performance, and the visualization of wake structures. Due to the uniqueness of the butterfly flight, the overall flight kinematics are evaluated by both wing and body kinematics. The aerodynamics performance

is analyzed based on instantaneous forces and power consumption. The wing-body coupling effects on the flight are presented by comparing the results between the original cases and wing-only cases.

A. Wing and body kinematics

Figure 4. (a) The time history of wing Euler angles. The gray shaded area represents downstroke period. t/T is the normalized transient time.(b) shows time history of the three wing Euler angle. The wing stroke angle has the amplitude of 148°, so the wings stroke from -95° to 52°. The lowest negative stroke angle exceeds -90° by 5°, which means, the wings clap together at the end of the upstroke, and the portions of wings that have not clapped yet maintain the upstroke motion for 5°. The wing pitch angle has the amplitude of 66°, which ranges from 68° to 134°. During the downstroke, the wing deviation is positive while it becomes negative at the mid upstroke. The amplitude of the deviation is roughly 25° which is small compared with the pitch and stroke angle.

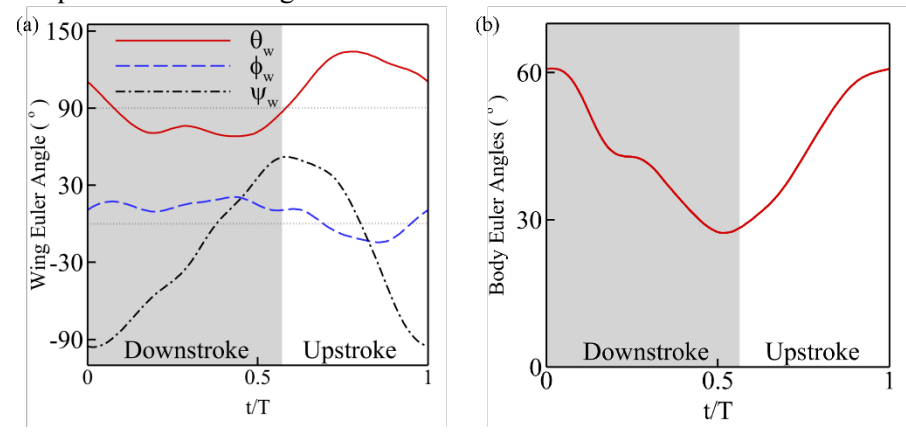


Figure 4. (a) The time history of wing Euler angles. The gray shaded area represents downstroke period. t/T is the normalized transient time. (b) The time history of the body pitch angle.

B. Aerodynamic performance

After solving the Navier-Stokes equations, the aerodynamic forces are obtained by the surface integration of pressure and shear stress over the wings and the body. The drag F_L and lift F_D are the vertical and horizontal force components, respectively. Figure 5a shows the instantaneous lift force produced by the left wing. The peak lift is produced during the downstroke. The lift is mainly produced during the downstroke and the lift in upstroke remains positive although the amount is small. The cycle-averaged lift is calculated by integrating the instantaneous lift over the period. During one flapping cycle, the cycle averaged lift produced by two wings of the original case is 8.37 mN. Besides, the flapping wing motion also induces flow on the body which can produce lift of 0.23mN. The results for both wings and body present sufficient lift to support the butterfly weight (8.53mN). The cycle average lift of the wing-only case is 8.26mN which is only 0.27 mN less than the original case and the wing-only case have similar trend as the original case. Although the lift forces between two cases are similar, the drag forces are different.

Figure 5b shows that, for both cases, the drag forces are positive during the downstroke and negative during the upstroke. The effective thrust forces for the forward flight are mainly produced by the upstroke. By comparison, the drag forces during the downstroke are similar for both cases. However, the thrust force, negative drag, of the original case is larger than that of the wing-only case. The cycle-averaged thrust of the original case is 10.44 mN and the one of the wing-only case is 9.26mN. The case with the existence of the body can produce 1.18mN more thrust, which is 12.74% more thrust.

As shown in Figure 5c, the mechanical power of both cases is close. The pattern of the power consumption in downstroke assembles the pattern of the instantaneous lift, and the upstroke power assembles the instantaneous thrust.

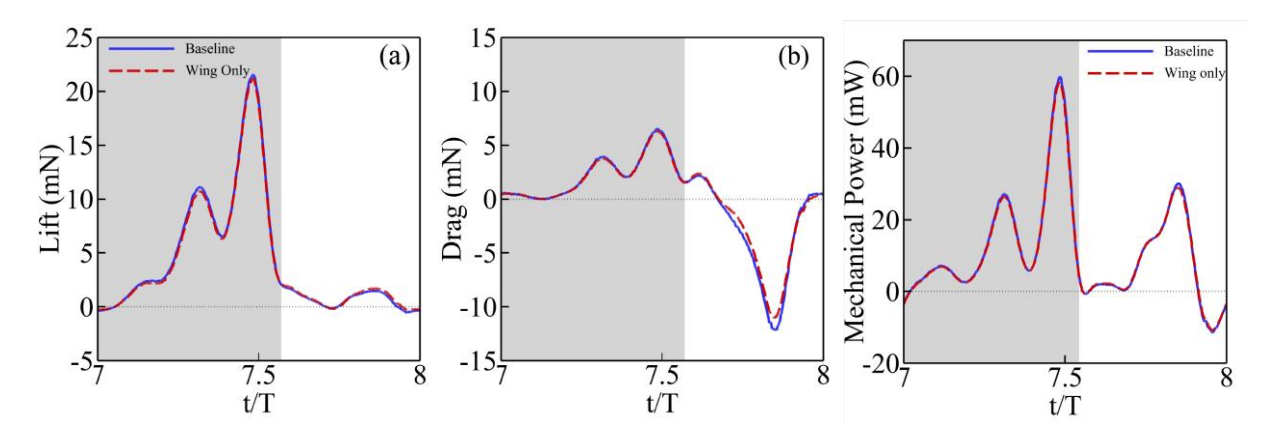


Figure 5. Time history of (a) the lift force, (b) the drag force and (c) the mechanical power consumption on wings

C. Wake structures

In Figure 6, the wake structures are visualized by Q-criterion and colored by the spanwise vorticity ω_z . At t/T = 7.625, we observed a vortex in the original case, but the same vortex structure was not generated in the wing-only case. Since the vortex is the result of the body and the body motion, the vortex results of the wing-body coupling. Such vortex was observed in other insects, such as the cicada, which is named as posterior body vortex (PBV).

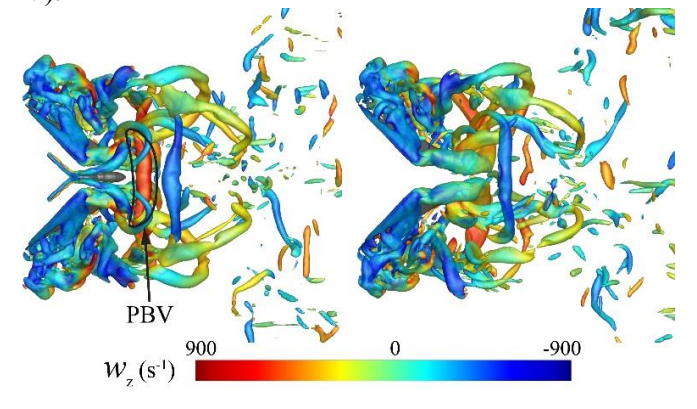


Figure 6. Vortex structure (Q-criterion) colored by the spanwise vorticity at t/T=7.625. The left is the baseline model and the right is the wings-only model.

To isolate the effect caused by the body, we ran a simulation for the body only with identical simulation conditions. As shown in Figure 7b and c, the body only case and wing only do not form PBV, which indicates that the PBV is not caused by the body pitching motion nor the flapping motion alone. Instead, the PBV is generated by the coupling effects of wing flapping motion and body. At t/T of 7.625, the mid of the upstroke, the PBV detached from the bottom of the abdomen. With the upstroke of the flapping motion, the PBV is then blow away as a jet.

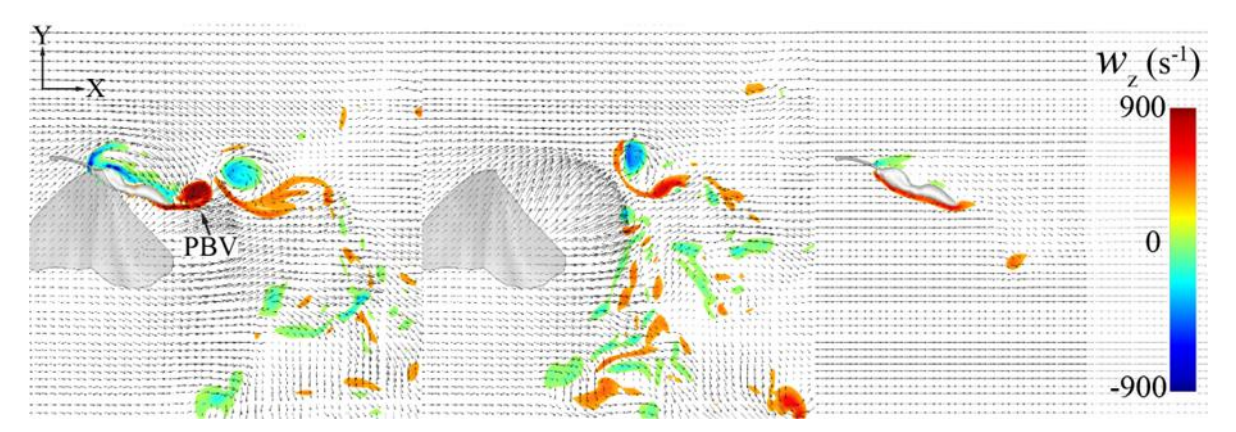


Figure 7. Cross-section of the velocity field and spanwise vorticity among (a) original case, (b) wing-only and (c) body-only model at t/T = 7.625.

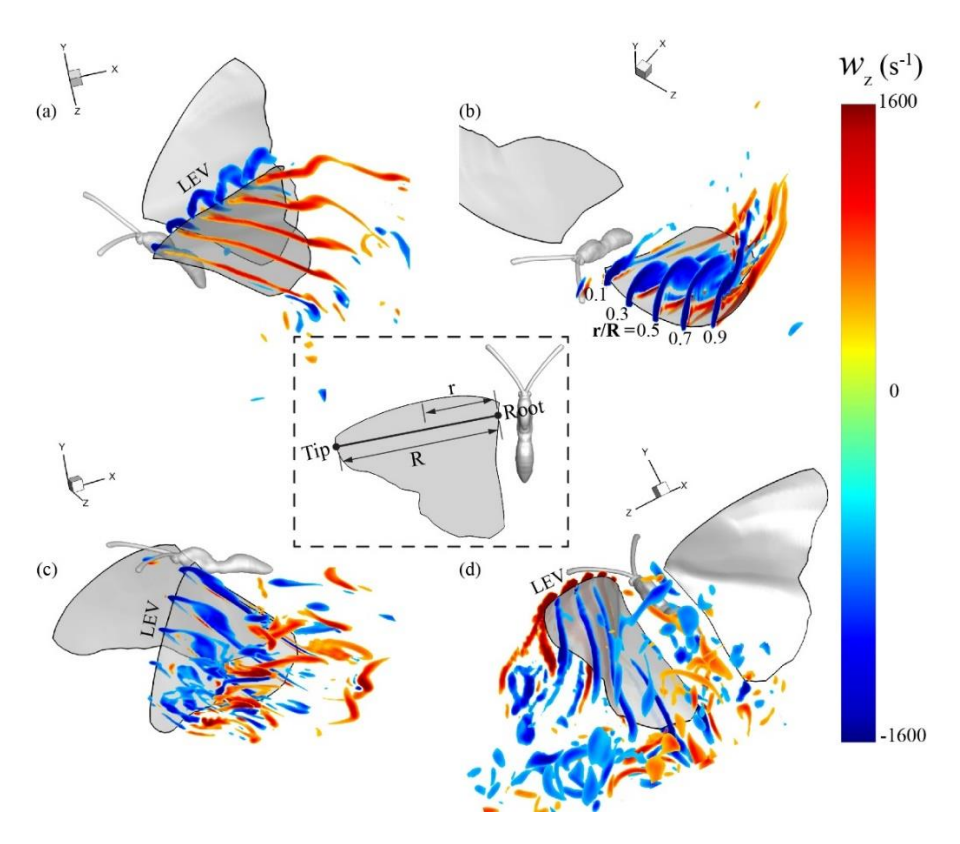


Figure 8. (a-d) Slicecut of wing vortex along the time sequence (t/T = t/T = 7.125, 7.375, 7.625, 7.875). r represents the distance from the slice to the root which depends on the slice location.

Figure 8 presents the leading-edge vortex (LEV) at four instants. We use r/R to describe the normalized the location regarding the wing root, so we cut five cross sections of the vorticity contour to evaluate the strength of LEV. The five slices are located at r/R of 0.1, 0.3, 0.5, 0.7, and 0.9. In Figure 8c, the distal two slice contour is weaker than the other three which indicates that the downstroke-generated LEV is weakened at t/T of 7.625, the mid upstroke.

To quantitatively present the development of the LEV, Figure 9a shows the distribution of the absolute circulation Γ of LEV at different time instance. Along the leading-edge, the circulation of LEV varies with time. We notice that the LEV is relatively stronger at r/R of 0.7 in general. This agrees with the common experimental observation of other insects that the LEV usually stays the strongest at 50% to 75% of the wingspan [31]. At this representative location of the leading-edge, r/R = 0.7, we present the instantaneous LEV circulation in one period in Figure 9b. Instead of the absolute circulation Γ , we show the signed values and the LEV circulation is all negative in the downstroke while the value become positive during the most upstroke. At roughly t/T = 7.625, the strength of LEV is too low, and the weakened vortices are difficult to identify. However, once the downstroke LEV dissipates, it only take about 5% of the period for the leadingedge to develop the upstroke LEV. The valley of curve iii in Figure 9a shows the weakened downstroke LEV at such moment, and the peak of curve iv shows the developed upstroke LEV after a quarter of the period. In a word, during the transition from the downstroke to the upstroke, the LEV will quickly dissipate from wing tip to wing root, and the upstroke motion will quickly develop a upstroke LEV within only 5% period. This fast procedure of gradually switching the LEV direction along the leading-edge continuously allows the sufficient circulation that attached to the leading-edge, so that the lift force is always sufficient to keep the butterfly aloft, namely 'delayed stall'.

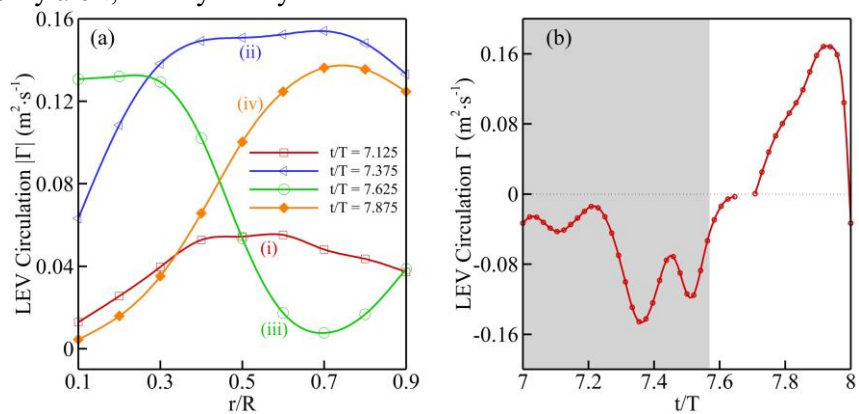


Figure 9. (a) The LEV circulation along the leading-edge at t/T=(i) 7.125, (ii) 7.375, (iii) 7.625 and (iv) 7.875. (b) The time history of LEV circulation at r/R=0.7.

Acknowledgments

The simulation work is supported by NSF CBET-2042368 and 2023 Villanova University Summer Grant Program to C. Li. All simulations were run on the High-Performance Computing Cluster of the College of Engineering at Villanova University.

References

- [1] Lentink, D., Dickson, W. B., Van Leeuwen, J. L., and Dickinson, M. H. "Leading-Edge Vortices Elevate Lift of Autorotating Plant Seeds." *Science*, Vol. 324, No. 5933, 2009, 1438–1440.
- [2] Stanford, B. K., and Beran, P. S. "Analytical Sensitivity Analysis of an Unsteady Vortex-Lattice Method for Flapping-Wing Optimization." *Journal of Aircraft*, Vol. 47, No. 2, 2010, 647–662.
- [3] Wu, J. H., and Sun, M. "Unsteady Aerodynamic Forces of a Flapping Wing." *Journal of Experimental Biology*, Vol. 207, No. 7, 2004, 1137–1150.

- [4] Dickinson, M. H., Lehmann, F. O., and Sane, S. P. "Wing Rotation and the Aerodynamic Basis of Insect Right." *Science*, Vol. 284, No. 5422, 1999, 1954–1960.
- [5] Sane, S. P. "Induced Airflow in Flying Insects I. A Theoretical Model of the Induced Flow." *Journal of Experimental Biology*, Vol. 209, No. 1, 2006, 34–42.
- [6] Lentink, D., and Dickinson, M. H. "Rotational Accelerations Stabilize Leading Edge Vortices on Revolving Fly Wings." *Journal of Experimental Biology*, Vol. 212, No. 16, 2009, 2705–2719.
- [7] Liu, G., Dong, H., and Li, C. "Vortex Dynamics and New Lift Enhancement Mechanism of Wing-Body Interaction in Insect Forward Flight." *Journal of Fluid Mechanics*, Vol. 795, 2016, 634–651.
- [8] Lee, K. B., Kim, J. H., Park, J. S., and Kim, C. "Unsteady Aerodynamic Effects of Wing-Body Interactions in Three-Dimensional Insects' Flapping Flight." 50th AIAA Aerospace Sciences Meeting Including the New Horizons Forum and Aerospace Exposition, No. January, 2012, 2012–0419.
- [9] Liang, B., and Sun, M. "Aerodynamic Interactions Between Wing and Body of a Model Insect in Forward Flight and Maneuvers." *Journal of Bionic Engineering*, Vol. 10, No. 1, 2013, 19–27.
- [10] Sridhar, M., Kang, C., and Landrum, D. B. "Beneficial Effect of the Coupled Wing-Body Dynamics on Power Consumption in Butterflies." *AIAA Aviation and Aeronautics Forum and Exposition, AIAA AVIATION Forum 2019*, No. January, 2019, 2019–0566.
- [11] Wan, H., Dong, H., and Gai, K. "Computational Investigation of Cicada Aerodynamics in Forward Flight." *Journal of the Royal Society Interface*, Vol. 12, No. 102, 2014.
- [12] Mittal, R., Dong, H., Bozkurttas, M., Najjar, F. M., Vargas, A., and von Loebbecke, A. "A Versatile Sharp Interface Immersed Boundary Method for Incompressible Flows with Complex Boundaries." *Journal of Computational Physics*, Vol. 227, No. 10, 2008, 4825–4852.
- [13] Li, C., Dong, H., and Zhao, K. "A Balance between Aerodynamic and Olfactory Performance during Flight in Drosophila." *Nature Communications*, Vol. 9, No. 1, 2018, 1–8.
- [14] Li, C. "Effects of Wing Pitch Kinematics on Both Aerodynamic and Olfactory Functions in an Upwind Surge." *Proceedings of the Institution of Mechanical Engineers, Part C: Journal of Mechanical Engineering Science*, Vol. 235, No. 2, 2021, 296–307.
- [15] Li, C., Dong, H., and Zhao, K. "Dual Functions of Insect Wings in an Odor-Guided Aeronautic Navigation." *Journal of Fluids Engineering*, Vol. 142, No. 3, 2020, 30902.
- [16] Liu, Y., Lozano, A. D., Hedrick, T. L., and Li, C. "Comparison of Experimental and Numerical Studies on the Flow Structures of Hovering Hawkmoths." *Journal of Fluids and Structures*, Vol. 107, 2021, 103405.
- [17] Lei, M., Crimaldi, J. P., and Li, C. "Navigation in Odor Plumes: How Do the Flapping Kinematics Modulate the Odor Landscape?" *AIAA Aviation and Aeronautics Forum and Exposition, AIAA AVIATION Forum 2021*, 2021, 2021–2817.
- [18] Lei, M., and Li, C. "The Aerodynamic Performance of Passive Wing Pitch in Hovering Flight." *Physics of Fluids*, Vol. 32, No. 5, 2020.

- [19] Lei, M., and Li, C. "A Balance Between Odor Intensity and Odor Perception Range in Odor-Guided Flapping Flight." *American Society of Mechanical Engineers, Fluids Engineering Division (Publication) FEDSM*, Vol. 2, 2022, 2022–85407.
- [20] Li, C., and Dong, H. "Three-Dimensional Wake Topology and Propulsive Performance of Low-Aspect-Ratio Pitching-Rolling Plates." *Physics of Fluids*, Vol. 28, No. 7, 2016.
- [21] Li, C., Dong, H., and Cheng, B. "Tip Vortices Formation and Evolution of Rotating Wings at Low Reynolds Numbers." *Physics of Fluids*, Vol. 32, No. 2, 2020, 021905.
- [22] Li, C., Wang, J., Liu, G., Deng, X., and Dong, H. "Passive Pitching Mechanism of Three-Dimensional Flapping Wings in Hovering Flight." *JSME-KSME 2019 8th Joint Fluids Engineering Conference*, Vol. 2, 2019, 2019–4639.
- [23] Justus, K. A., Schofield, S. W., Murlis, J., and Cardé, R. T. "Flight Behaviour of Cadra Cautella Males in Rapidly Pulsed Pheromone Plumes." *Physiological Entomology*, Vol. 27, No. 1, 2002, 58–66.
- [24] Xu, M., Wei, M., Li, C., and Dong, H. "Adjoint-Based Optimization for Thrust Performance of Three-Dimensional Pitching-Rolling Plate." *AIAA Journal*, Vol. 57, No. 9, 2019, 3716–3727.
- [25] Lei, M., Crimaldi, J. P., and Li, C. "Navigation in Odor Plumes: How Do the Flapping Kinematics Modulate the Odor Landscape?" *AIAA Aviation 2019 Forum*, 2021, 2021–2817.
- [26] Li, C., Dong, H., and Liu, G. "Effects of a Dynamic Trailing-Edge Flap on the Aerodynamic Performance and Flow Structures in Hovering Flight." *Journal of Fluids and Structures*, Vol. 58, 2015, 49–65.
- [27] Li, C., and Dong, H. "Wing Kinematics Measurement and Aerodynamics of a Dragonfly in Turning Flight." *Bioinspiration and Biomimetics*, Vol. 12, No. 2, 2017.
- [28] Li, C., Jiang, J., Dong, H., and Zhao, K. "Computational Modeling and Validation of Human Nasal Airflow under Various Breathing Conditions." *Journal of Biomechanics*, Vol. 64, 2017, 59–68.
- [29] Lionetti, S., Hedrick, T. L., and Li, C. "Aerodynamic Explanation of Flight Speed Limits in Hawkmoth-like Flapping-Wing Insects." *Physical Review Fluids*, Vol. 093104, 2022, 1–24.
- [30] Lei, M., and Li, C. "Numerical Investigation of the Passive Pitching Mechanism in Odor-Tracking Flights." *AIAA Aviation 2020 Forum*, Vol. 1 PartF, 2020, 2020–3016.
- [31] Birch, J. M., and Dickinson, M. H. "Spanwise Flow and the Attachment of the Leading-Edge Vortex on Insect Wings." *Nature*, Vol. 412, No. 6848, 2001, 729–733.